Chinese Chemical Letters 35 (2024) 109467

Contents lists available at ScienceDirect

Chinese Chemical Letters

journal homepage: www.elsevier.com/locate/cclet

Sulphur-template method for facile manufacturing porous silicon electrodes with enhanced electrochemical performance

Peng Zhou, Ziang Jiang, Yang Li, Peng Xiao*, Feixiang Wu*

Powder Metallurgy Research Institute, School of Metallurgy and Environment, Central South University, Changsha 410083, China

ARTICLE INFO

Article history:
Received 27 November 2023
Revised 12 December 2023
Accepted 26 December 2023
Available online 5 January 2024

Keywords:
Sulphur-template
Porous electrodes
Silicon anodes
Low volume expansion
Lithium-ion batteries

ABSTRACT

Sulphur (S)-template method based on conventional slurry-casting method has been developed to produce porous silicon (Si) electrodes. The facile fabrication technology is suitable for current production line and expected to be widely applied to various electrode materials under large volume change during operation. Specifically, S particles as template agent are mixed with active material Si, carbon conductor and binder forming uniform slurry. After casting and drying, the electrodes are immersed in carbon disulfide solution to remove S particles rapidly, generating pores *in-situ* at the original position of S particles. Electrochemical analysis shows that the pores inside electrodes are able to shorten lithium ion diffusion paths, reduce normal expansion rate and decrease formation of cracks in the Si electrode (2 mg_{Si}/cm^2), demonstrating a reversible capacity of 951 mAh/g at 0.5 A/g after 100 cycles (with a capacity retention of 99.5%) and a capacity of ~826 mAh/g at 2 A/g.

To meet the growing energy demands, numerous researchers devote themselves to develop light and portable storage batteries [1]. Alloying-type electrode materials for lithium ion batteries (LIBs) have been attracting extensive attention due to their high gravimetric and volumetric capacity, such as Si, Al, GeS and SnS [2–6]. However, alloying-type electrode materials show dramatic volume change during cycling, which results in the generation of cracks along the electrodes and subsequently exfoliation of active materials away from current collectors [7]. Therefore, alloying-type electrodes tend to show poor cycling stability and are difficultly applied in markets [8]. To overcome the issues mentioned above, most of studies proposed designs on new structures at the scale of a single particle, such as core-shell structures [9,10], yolk-shell structures [11,12] or build integrated 3-dimentional structures [13,14]. However, the solutions mentioned above are not suitable for various alloying-type electrode materials because of complex fabrication technologies and different physical and chemical properties of different matrixes.

Rolling, a traditional procedure during electrode preparation following mixing slurry, casting and drying, is aimed to decrease porosity, increase tap density, and improve electrochemical performances of insertion-type electrodes with inconspicuous volume change rate. Instead, as for alloying-type electrodes, rolling might be not suitable. Even more, appropriate pores introduced inside the electrodes are hoped to accommodate the huge expansions of alloying-type electrode materials during cycling. As a result, we innovatively develop a new facile technology, namely template-method, to generate pores inside the electrodes. Specifically, templates are introduced inside the electrodes and subsequently removed to *in-situ* generate appropriate pores at the original position of the templates inside the electrodes. Compared with the present production line, this method does not change much except for the procedure of removing templates. Therefore, template-method is much more possible to be applied to prepare high-performance porous alloying-type electrodes for mass production.

Silicon (Si) is one of the alloying-type anode materials and possesses extensive application potentials [15,16]. In this paper, micro-sized sulphur (S) particles as template agent are added during the process of mixing slurry, and subsequently washed away using carbon disulfide (CS_2) to generate pores at the original position of S particles inside Si anodes. In half-cell tests, the porous Si electrodes show enhancing cycling life and excellent rate performance compared to normal Si electrodes due to lower expansion rate of electrodes, lower over-potential and faster lithium-ion (Li^+) diffusion rate. The porous Si electrodes at a high loading of about 2 $mg_{(Si)}/cm^2$ offer reversible capacity of 951 mAh/g after 100 cycles at 0.5 A/g with a capacity retention of 99.5% and high re-

* Corresponding authors.
E-mail addresses: xiaopeng@csu.edu.cn (P. Xiao), feixiang.wu@csu.edu.cn (F. Wu).

https://doi.org/10.1016/j.cclet.2023.109467
1001-8417/

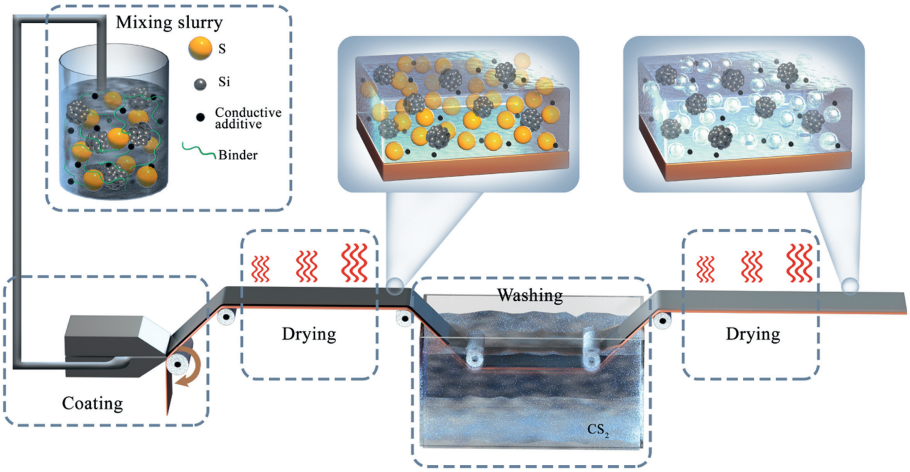

Fig. 1. The schematic illustration of porous electrodes *via* the modified slurry-casting method.

versible capacity of 825.9 mAh/g at 2 A/g. Furthermore, the pores inside the porous electrodes are able to facilitate the Li^+ diffusion and show promising electrochemical performances. Therefore, the template method can be applied to produce high-loading porous electrodes including a series of cathodes and anodes in mass production when appropriate template and corresponding solvent moving away the templates are utilized.

Traditional slurry-casting method is used to fabricate porous Si electrodes but further modified with an additional succeeding process that using CS_2 to dissolve S particles as a template. The schematic illustration of porous electrodes *via* the modified slurry-casting method is shown in Fig. 1. Typically, S particles mix with active material Si, conductive additive and binder in solution to fabricate slurry cast on the carbon-coated Cu foil. After absolutely dried, the pristine electrodes are immersed in CS_2 to move away S particles and *in-situ* fabricate pores inside the electrodes. After volatilization of CS_2 in ambient temperature, the porous Si electrodes are prepared.

The surface morphology and phase constitution of the porous Si electrodes before and after being washed using CS_2 are displayed in Fig. 2. As shown in Fig. 2a, the pristine electrodes before being washed by CS_2 are relatively flat. The bright part of the SEM image is S particles caused by intensive electron charging as a result of the relatively poorer electricity conductivity of S [17]. The EDS element mapping (Fig. 2b) of Fig. 2a illustrates that the bright part of the SEM image is S particles, which evenly distribute inside the pristine electrodes. The SEM image and particle size distribution of S particles are shown in Fig. 2f. The average particle size of S particles is 25.3 μm. S particles can rapidly dissolve in CS_2 for half a minute. After the pristine electrodes are washed using CS_2, plenty of pores *in-situ* generate inside the porous electrodes at the original position of S particles (Figs. 2c and e) and no S can be observed by the EDS element mapping image (Fig. 2d) of Fig. 2c. The Si and S element weight ratio of pristine electrode and porous electrode are shown in Fig. 2h. XRD is conducted to further identify that the S particles are totally moved away by CS_2. As shown in Fig. 2g, the pristine electrodes show intense XRD peaks of S. After being washed by CS_2, the electrodes only show the XRD peaks of active material Si and current collector Cu, which also illustrates S particles are totally moved away by CS_2 and no other side reactions occurs.

The electrochemical performances of Si electrodes and porous Si electrodes at different Si loadings are shown in Fig. 3. The initial galvanostatic charge/discharge curves between 0.01 V and 3.0 V (*vs.* Li/Li^+) of Si electrodes and porous Si electrodes at 0.1 A/g are shown in Fig. 3a. Si electrodes show lithiation capacity, delithiation capacity and initial Coulombic efficiency (ICE) of 1492.4 mAh/g, 947.3 mAh/g and 63.5%, respectively, while the porous Si electrodes exhibit those of 2024.8 mAh/g, 1284.9 mAh/g and 63.5%, respectively. The results reveal the pores inside the porous Si electrodes can increase the utilization rate of active Si but barely change the ICE. Fig. 3b illustrates the locally magnified curves of Fig. 3a in potential window between 0 V and 0.3 V (*vs.* Li/Li^+). Over-potential is caused by the polarization of electrode impacted by Li^+ diffusion, resistance and so on [18]. Si electrodes exhibit obviously higher over-potential of 53.3 mV than that of 38.5 mV for the porous Si electrodes. That reveals the pores inside the porous Si electrodes can reduce over-potential, which is beneficial from the improvement of Li^+ diffusion rate (Fig. S1 in Supporting information). Fig. 3c displays the galvanostatic charge/discharge cycling curves of Si electrodes and porous Si electrodes at 0.5 A/g after initial three cycles at 0.1 A/g, respectively. The capacity retention (after 103 cycles at 0.5 A/g compared with the 4^{th} cycle) of the porous Si electrodes of 99.5% is remarkably higher than that of Si electrodes of 73.5%. The outstanding cycle stability of the porous Si electrodes may be ascribed to a lower normal expansion rate of electrode due to that pores inside the porous Si electrodes are able to accommodate the expansion of lithiated Si. Fig. 3d demonstrates the rate performances of Si electrodes and porous Si electrodes, respectively. The porous Si electrodes show more excellent rate capability than Si electrodes. The porous Si electrodes exhibit reversible capacities of 1688, 1615, 1339, 1057 and 745 mAh/g at a variety of current density of 0.1, 0.2, 0.5, 1 and 2 A/g, respectively, and when the current returns to 0.5 A/g, a reversible capacity of 1412 mAh/g is recovered. Figs. 3e and f illustrate the charge/discharge curves of the Si electrodes and porous Si electrodes at various current densities over the voltage window of 0.01–1.5 V, respectively. Notably, the voltage plateau of the charge–discharge process in Si electrodes and porous Si electrodes increases/decreases as the current density increases. It is noted the increase/decrease of charge/discharge voltage plateau is slower in porous Si electrodes than Si electrodes, indicating a smaller electrochemical polarization in porous Si electrodes. The excellent rate capability of the porous Si electrodes attribute to the pores inside the electrodes shortening the Li^+ diffusion paths resulting in small electrochemical polarization.

To further demonstrate the outstanding electrochemical performances of porous Si electrodes, the electrode kinetics of Si electrodes and porous Si electrodes is investigated through CV curves

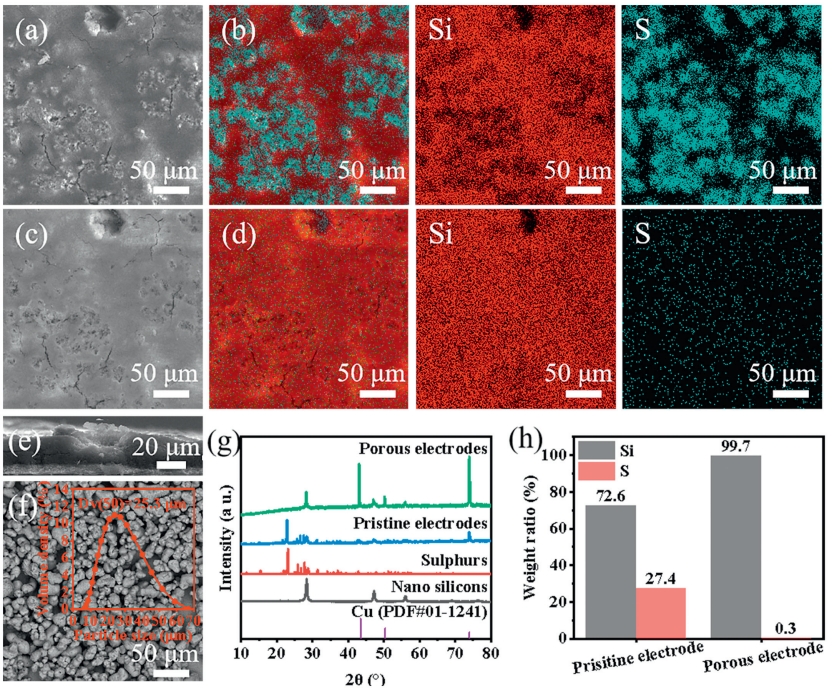

Fig. 2. *In-situ* SEM images of porous Si electrodes: (a) Before and (c) after washing away S particles using CS_2. Element mapping images: (b) Before and (d) after washing away S particles using CS_2. (e) Cross-section SEM image of porous Si electrodes. (f) SEM image of S particles (inset: particle size distribution of S particles). (g) XRD patterns of porous Si electrodes before and after washing sulphur particles using CS_2. (h) Si and S element weight ratio of pristine electrode and porous electrode.

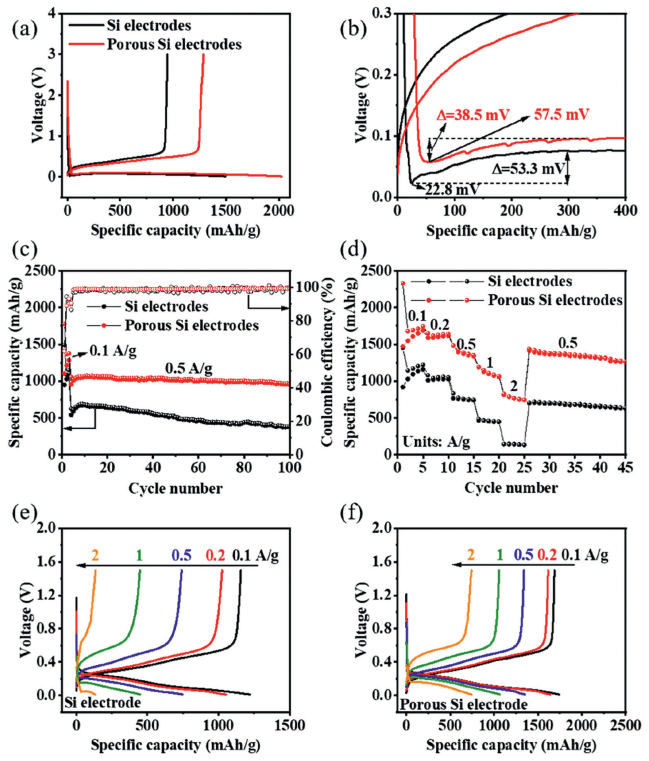

Fig. 3. (a) Initial charge/discharge curves. (b) Locally magnified curves of (a). (c) Charge/discharge cycling performances and corresponding coulombic efficiency at 0.5 A/g after initial three 0.1 A/g. (d) Rate performances of Si electrodes and porous Si electrodes. Charge/discharge curves of (e) Si electrode and (f) porous Si electrodes at various current densities from 0.1 A/g to 2 A/g.

(Figs. S1a and b). The maximum anodic current linearly increased with the square root of ν when different scan rates (ν) (0.1–1.0 mV/s) were applied, indicating a diffusion-controlled process [19]. The Li^+ diffusion coefficient (D_{Li^+}) of Si-based anodes was calculated using the Randles–Sevcik relation from a plot of the maximum current peak (I_p) *versus* the square root of ν (Fig. S1c) [20]. The equation is as follows,

$$I_p = 2.69 \times 10^5 n^{3/2} A D_{Li^+}^{1/2} \nu^{1/2} C_{Li^+} \quad (1)$$

where $I_p/\nu^{1/2}$ is slope obtained from Fig. S1c, n represents transfer number of electrons per molecule during the conversion reaction ($n = 1$), A is electrode surface area and C_{Li^+} symbolizes molar concentration of Li^+. The D_{Li^+} of porous Si electrode of 3.2×10^{-13} cm/s is notably higher than that of Si electrode of 2.0×10^{-14} cm/s. The results above illustrate that the pores inside the electrodes are capable of improving the sluggish kinetics of thick electrodes.

To demonstrate the excellent electrochemical performances of porous Si electrodes, the SEM morphology and photograph of Si electrodes and porous Si electrodes before and after 100 cycles are shown in Fig. 4. The thickness of the cross-section of Si electrodes and porous Si electrodes is shown in Figs. 4a, b, f, g. It is calculated that expansion rate of Si electrodes and porous Si electrodes is 78.5% and 45.8%, respectively, indicating that the presence of pores inside the electrodes can effectively inhibit volume expansion of the electrode. Before cycling, the surface of the electrodes is relatively flat (Figs. 4c and h). After 100 cycles, most active material Si has exfoliated from current collector in Si electrodes (Fig. 4e) while active material Si are well coated on current collector in porous Si electrodes (Fig. 4j). Surface SEM image show straight, long and wide cracks in Si electrodes (Fig. 4d) while crooked, short and narrow cracks in porous Si electrodes (Fig. 4i). That is ascribed to the huge volume expansion of Si particles, easily caus-

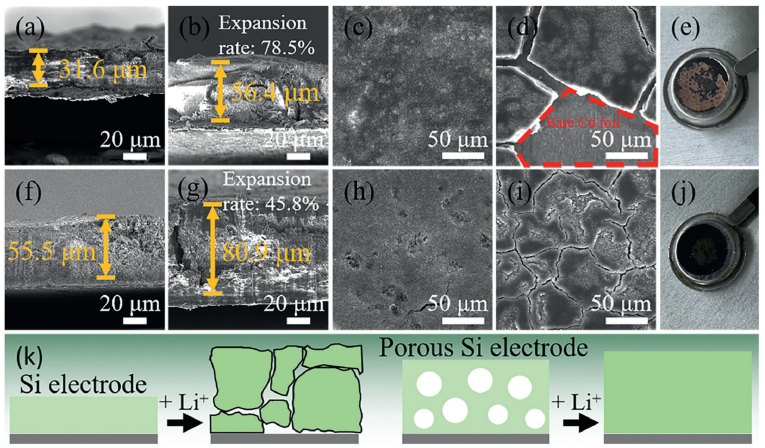

Fig. 4. SEM images of (a–d) Si electrodes and (f–i) porous Si electrodes (a, c, f, h) before cycling and (b, d, g, i) after 100 cycles: (a, b, f, g) cross-section images and (c, d, h, i) surface images. Photograph of (e) Si electrodes and (j) porous Si electrodes after 100 cycles. (k) Schematic illustration showing the morphology evolution of Si electrodes and porous Si electrodes after cycling.

ing stress concentration of Si anodes. During lithiation procedure, the lithiated silicons fill the pores (Fig. 4h) and decrease normal expansion rate, which is beneficial for the improvement of cycle stability of porous Si electrodes. The corresponding schematic illustration showing the morphology evolution of Si electrodes and porous Si electrodes after cycling is shown in Fig. 4k.

A novel modified slurry-casting method was developed to produce porous Si electrodes. These porous configurations not only accelerate Li^+ diffusion, reducing polarization and enabling high-loading electrodes, but also augment the energy density of LIBs. Crucially, the inherent porosity counteracts the substantial volume expansion of Si during lithiation, thus reducing cracks and improving the electrodes' cycle stability. Our innovative template-based approach allows for customization of pore attributes, adjusting their quantity, shape and size as per requirements. The method's adaptability for mass production is underscored by its compatibility with various templates and corresponding solvents. Beyond addressing thick electrode kinetics, this technique offers a solution to the significant volume expansion characteristic of alloying-type electrodes. In essence, the modified slurry-casting method presents itself as a promising contender for broader electrode fabrication applications.

Declaration of competing interest

The authors declare that they have no known competing financial interests or personal relationships that could have appeared to influence the work reported in this paper.

Acknowledgments

The authors gratefully acknowledge the National Natural Science Foundation of China (Nos. 51904344 and 52172264) and the Natural Science Foundation of Hunan Province of China (Nos. 2021JJ10060 and 2022GK2033).

Supplementary materials

Supplementary material associated with this article can be found, in the online version, at doi:10.1016/j.cclet.2023.109467.

References

[1] M. Armand, J.M. Tarascon, Nature 451 (2008) 652–657.
[2] D. Chao, B. Ouyang, P. Liang, et al., Adv. Mater. 30 (2018) 1804833.
[3] J.W. Choi, D. Aurbach, Nat. Rev. Mater. 1 (2016) 16013.
[4] D. Li, F. Chu, Z. He, et al., Mater. Today 58 (2022) 80–90.
[5] G.K. Sung, C.M. Park, J. Mater. Chem. A 5 (2017) 5685–5689.
[6] B. Wang, J. Ryu, S. Choi, et al., ACS Nano 13 (2019) 2307–2315.
[7] D. Zhang, J. Lu, C. Pei, et al., Adv. Energy Mater. 12 (2022) 2103689.
[8] Q. Man, Y. An, C. Liu, et al., J. Energy Chem. 76 (2023) 576–600.
[9] D. Chao, X. Xia, J. Liu, et al., Adv. Mater. 26 (2014) 5794–5800.
[10] Z. Yao, X. Xia, C.A. Zhou, et al., Adv. Sci. 5 (2018) 1700786.
[11] R. Mo, D. Rooney, K. Sun, et al., Nat. Commun. 8 (2017) 13949.
[12] X. Shi, Y. Gan, Q. Zhang, et al., Adv. Mater. 33 (2021) 2100837.
[13] J. Ji, H. Ji, L.L. Zhang, et al., Adv. Mater. 25 (2013) 4673–4677.
[14] H. Shang, Z. Zuo, L. Yu, et al., Adv. Mater. 30 (2018) 1801459.
[15] L. Liu, B. Wu, J. Tao, et al., Adv. Compos. Hybrid Mater. 5 (2022) 3002–3011.
[16] J. Tao, L. Liu, J. Han, et al., Energy Storage Mater. 60 (2023) 102809.
[17] K. Chansoon, C.Y. Whan, J. Power Sources 485 (2021) 229311.
[18] N. Qin, L. Jin, G. Xing, et al., Adv. Energy Mater. 13 (2023) 2204077.
[19] Y.T. Malik, S.Y. Shin, J.I. Jang, et al., Small 19 (2023) 2206141.
[20] Y. Son, S. Sim, H. Ma, et al., Adv. Mater. 30 (2018) 1705.